



# Monitoring tumour microenvironment changes during anti-angiogenesis therapy using functional MRI

Jianye Liang<sup>1</sup> · Qingqing Cheng<sup>1</sup> · Jiaxi Huang<sup>1</sup> · Mengjie Ma<sup>1</sup> · Dong Zhang<sup>1</sup> · Xueping Lei<sup>3</sup> · Zeyu Xiao<sup>1</sup> · Dongmei Zhang<sup>2</sup> · Changzheng Shi<sup>1</sup> · Liangping Luo<sup>1</sup>

Received: 26 February 2019 / Accepted: 16 May 2019 / Published online: 30 May 2019  
© Springer Nature B.V. 2019

## Abstract

**Objective** This study aims to explore the feasibility of dynamic contrast-enhanced magnetic resonance imaging (DCE-MRI) and blood oxygen level-dependent magnetic resonance imaging (BOLD-MRI) in assessing vessel function and tumour aggressiveness during anti-angiogenesis treatment.

**Materials and methods** A colon cancer xenograft model was established in BALB/C nude mice with the HCT116 cell line. Sixteen mice were randomly divided into Group A and Group B, which were treated with saline or bevacizumab by intraperitoneal injection on the 1st, 4th, 7th, 10th and 13th days and underwent DCE-MRI and BOLD-MRI examinations before and on the 3rd, 6th, 9th, 12th and 15th days after treatment. Group C was treated with oxaliplatin monotherapy, and Group D was treated with bevacizumab and oxaliplatin as a point of comparison for therapeutic effects. The pathological examinations included HE, HIF-1 $\alpha$ , fibronectin and TUNEL staining, as well as  $\alpha$ -SMA and CD31 double staining. One-way analysis of variance and correlation analysis were the main methods used for statistical analysis.

**Results** Group D manifested the highest tumour inhibition rate and smallest tumour volume on day 15, followed by Group C, Group B and Group A.  $K_{trans}$  ( $F=81.386$ ,  $P<0.001$ ),  $K_{ep}$  ( $F=45.901$ ,  $P<0.001$ ),  $V_e$  ( $F=384.290$ ,  $P<0.001$ ) and  $R2^*$  values ( $F=89.323$ ,  $P<0.001$ ) showed meaningful trends with time in Group B but not Group A. The  $K_{trans}$  values and tumour vessel maturity index (VMI) were higher than baseline values 3–12 days after bevacizumab treatment. The CD31 positive staining rate and VMI had the strongest correlations with  $K_{trans}$  values, followed by  $AUC_{180}$ ,  $V_e$  and  $K_{ep}$  values. The  $R2^*$  value positively correlated with the positive staining rates of HIF-1 $\alpha$  and fibronectin.

**Conclusion** Intermittent application of low-dose anti-angiogenic inhibitor treatment may help improve the effect of chemotherapy by reducing hypoxia-related treatment resistance and improving drug delivery. DCE-MRI is useful for evaluating vessel maturity and vascular normalization, while BOLD-MRI may help to predict tumour hypoxia and metastatic potential after anti-vascular treatment.

**Keywords** DCE-MRI · BOLD-MRI · Anti-angiogenesis treatment · Vascular normalization · Hypoxia

---

Jianye Liang and Qingqing Cheng have contributed equally to this work.

**Electronic supplementary material** The online version of this article (<https://doi.org/10.1007/s10456-019-09670-4>) contains supplementary material, which is available to authorized users.

- 
- ✉ Dongmei Zhang  
dmzhang701@jnu.edu.cn
  - ✉ Changzheng Shi  
tsczc@jnu.edu.cn
  - ✉ Liangping Luo  
tluolp@jnu.edu.cn

Extended author information available on the last page of the article

## Introduction

Tumour growth, invasion and metastasis are closely related to tumour angiogenesis. A hypoxic microenvironment is one of the important characteristics of solid tumours and is commonly observed in aggressive tumours when even the newly generated vessels are insufficient to provide the required oxygen for tumour growth. Hypoxia can promote cell differentiation, inhibit cell proliferation and induce cell apoptosis and tumour necrosis. However, adaptive changes, including the upregulation of angiogenic factors (e.g. VEGF, PDGF-B and TGF- $\beta$ ), which could stimulate the formation of tumour vessels, may occur when the tumours undergo a

long period of hypoxia. The newly generated tumour vessels are generally tortuous, disorganised, highly permeable and characterised by abnormalities in their endothelial wall, pericyte coverage and basement membrane. Vascular endothelial growth factor A (VEGF-A) is a major permeability and pro-angiogenic factor that is highly expressed during tumour growth. A direct consequence of VEGF-induced vessel leakiness is increased interstitial fluid pressure and forms a barrier to oxygen delivery. In addition, the highly proliferative and dense tumour cells can compress and destabilise the surrounding blood vessels, which can lead to vessel regression and reduced tumour perfusion and further aggravate the tumour hypoxia [1]. The hypoxic microenvironment can drive the transformation of tumour cells from proliferative to invasive phenotypes and promote the expression of the hypoxia-inducible factor 1 $\alpha$  (HIF-1 $\alpha$ ) gene, which could induce epithelial–mesenchymal transition in tumour cells [2]. The tumour may express a variety of mesenchymal cell-associated proteins (e.g. vimentin and N-cadherin) and decrease the expression of fibronectin. These aggressive mesenchymal phenotypes further enhance the invasion and migration ability of tumours [3]. Most importantly, hypoxia can mediate chemoresistance and radioresistance [4], which urges the exploration of a newly targeted mechanism for anti-tumour treatment. On the other hand, the high vascular permeability and increased interstitial fluid pressure, which may hamper delivery of chemotherapeutic drugs to the tumour, need to be addressed. Bevacizumab is a recombinant human monoclonal IgG antibody that specifically binds to VEGF-A and prevents it from interacting with its receptors (VEGFR1 and 2). It was originally used to reduce tumour neovascularization and inhibit tumour growth [5]. Anti-angiogenic therapy is an important component of current cancer treatment, but there is still some controversy because excessive inhibition of neovascularization will aggravate tumour hypoxia and further impede drug delivery, whereas recent studies reported that anti-angiogenic therapy can temporarily normalise the vessel structure and function [6], which may increase the tumour blood supply and ameliorate hypoxia, helping to address current treatment dilemmas. However, the time ranges of the vascular normalization process are still inconsistent due to a variety of evaluation criteria. In addition, the ideal treatment dosage to balance the anti-angiogenic effect and vascular normalization phenomenon is still an interesting topic.

Aside from the above issues, how to effectively monitor the tumour perfusion, hypoxic degree and other microenvironmental changes during anti-vascular treatment is another important issue, which will help to evaluate the treatment effect and determine the vascular normalization process convincingly. In a recent animal study, Pan et al. [7] found that intravoxel-incoherent-motion diffusion-weighted imaging (IVIM-DWI) has the potential to serve as a non-invasive

approach for monitoring Endostar-induced tumour vascular normalization without the need for contrast agents. However, it cannot mimic the process of drug delivery and is not suitable for our study. Dynamic contrast-enhanced magnetic resonance imaging (DCE-MRI) is a non-invasive imaging method that can reflect the characteristics of tumour microvasculature and has been widely used in both experimental and clinical pharmacological studies [8–10]. It can quantitatively measure tumour perfusion and vascular permeability, which is suitable for current anti-vascular studies. In addition, the transport of contrast agent mimics the process of drug delivery, which is more convincing than non-enhanced IVIM-DWI. Blood oxygen level-dependent magnetic resonance imaging (BOLD-MRI) is another advanced imaging sequence that is sensitive to iron deposition and deoxyhemoglobin concentration in the microenvironment. The accumulation of deoxyhemoglobin, which is a paramagnetic material, may interfere with the uniformity of the magnetic field and accelerate the dephasing process of T2\* relaxation and cause an increase in R2\* values. It can indirectly reflect oxygen metabolism [11] and is suitable to measure tumour hypoxia during anti-vascular therapy.

Previously, few studies have been concerned with continuously monitoring the microenvironment changes during anti-vascular therapy using functional MRI, especially the phenomenon of vascular normalization. Oxaliplatin is a common chemotherapeutic drug for colon cancer, and the combination with anti-angiogenic drugs has shown improved therapeutic effect in clinical studies [12]. However, the mechanisms are not well investigated. Illuminating the potential anti-tumour mechanisms and microenvironment changes (e.g. tumour perfusion, hypoxia and migration ability) has important clinical implications for combined chemotherapy. In this study, we used DCE-MRI and BOLD-MRI to continuously monitor changes in the microenvironment in a colon cancer xenograft model and investigate the synergistic effect of bevacizumab when combined with chemotherapeutic drugs such as oxaliplatin during anti-vascular treatment. The outcomes may address these issues and guide optimal anti-tumour treatment.

## Materials and methods

### Cell culture

We obtained the human colon cancer HCT116 cell lines from the American Type Culture Collection (ATCC, Manassas, Virginia). They were cultured in Dulbecco's modified Eagle's medium (DMEM, Gibco) supplemented with 10% foetal bovine serum and 1% penicillin/streptomycin and maintained at 37 °C in a 5% CO<sub>2</sub> atmosphere.

## Tumour model and grouping

This animal experiment was approved by the Institutional Animal Ethics Committee of our university. We strictly followed the Institutional Laboratory Animal Care and Use Manual. A total of 105 female BALB/c nude mice, aged 6–7 weeks and weighing approximately 15–20 g, were purchased from Beijing Vital River Laboratory Animal Technology Corporation (Certificate Nos. 11400700325797 and 11401500046283, China). The mice were subcutaneously injected with 0.2 ml of  $1 \times 10^6$ /ml HCT116 cells into the right flank near the hindlimbs to establish the colon cancer xenograft model and were raised in a specific pathogen-free environment. The experiments were initiated 2 weeks after implantation as the mean tumour volume reached approximately  $200 \text{ mm}^3$ , which allowed the tumours to maintain a rapid growth stage with relatively high vascularity and without significant necrosis and was the best opportunity to monitor the treatment effect and microenvironment changes.

We selected 83 tumour-bearing mice for the experiment. Sixteen mice were randomly divided into Group A and Group B (eight for each), which were treated with saline or bevacizumab (avastin, Roche, Switzerland), and underwent DCE-MRI and BOLD-MRI examinations before and on the 3rd, 6th, 9th, 12th and 15th day after treatment. Group C ( $n=8$ ) treated with oxaliplatin monotherapy (4 mg/kg, dissolved in 5% glucose solution), and Group D ( $n=8$ ) treated with bevacizumab and oxaliplatin were also set for therapeutic effect comparison. All mice were treated by intraperitoneal injection on the 1st, 4th, 7th, 10th and 13th days. Distinct from a previous study [13], we repeatedly used a relatively low dose of bevacizumab (5 mg/kg) this time. As bevacizumab was diluted with 0.9% normal saline, it was injected 1 h before oxaliplatin administration to avoid drug interaction in Group D. The short diameter (a) and long diameter (b) of the tumour were measured with callipers on days 0, 3, 6, 9, 12 and 15 after treatment. The tumour volume was calculated as  $(a^2 \times b \times 0.5) \text{ mm}^3$ . The tumour inhibition rate was calculated as  $(\text{tumour volume of control group} - \text{tumour volume of treatment group}) / \text{tumour volume of control group} \times 100\%$ .

## MRI examinations

Animals were anaesthetised by intraperitoneal injection of 0.1% pentobarbital sodium before imaging. MR examination was performed on a 1.5 T Signa HDxt superconductor clinical MR system (GE Medical System, Milwaukee, WI) equipped with a special animal coil. They were imaged in the supine position. Conventional T1-weighted images (T1WI) were acquired using fast spin-echo (FSE) sequences with the following parameters: repetition time/echo time (TR/TE) = 540/14.7 ms, slice thickness = 2 mm,

slice gap = 0.2 mm, field of view (FOV) =  $5 \times 5 \text{ cm}^2$ , matrix size =  $192 \times 160$ , number of excitations (NEX) = 2. T2-weighted images (T2WI) were acquired using fast recovery fast spin-echo sequences with the following parameters: TR/TE = 2140/82.3 ms, slice thickness = 2 mm, slice gap = 0.2 mm, FOV =  $5 \times 5 \text{ cm}^2$ , matrix size =  $192 \times 160$  and NEX = 2. BOLD-MRI was performed with a three-dimensional spoiled gradient echo sequence and the following parameters were used: sixteen TEs (TE = 3.4, 9.3, 15.2, 21.2, 27.1, 33, 38.9, 44.8, 50.7, 56.6, 62.5, 68.5, 74.4, 80.3, 86.2, 92.1), TR = 160 ms, FOV =  $8.0 \times 6.4 \text{ cm}^2$ , matrix size =  $192 \times 128$  and NEX = 2. The mice were imaged in free-breathing, so the air in a normal oxygen level was used for BOLD-MRI. DCE-MRI was performed with the fast spoiled gradient-recalled echo (SPGR) sequence with the following parameters: TR = 40 ms, TE = 2.4 ms, slice thickness = 2 mm, slice gap = 0.2 mm, matrix size =  $128 \times 96$  and FOV =  $7.0 \times 5.6 \text{ cm}^2$ . The mice were catheterised and manually administered 0.1 mmol/kg Gd-DTPA (Magnevist®, Bayer Schering Pharma, Germany) via the tail vein in approximately 5 s, followed by 0.3 ml of a 0.9% saline flush before scanning. A total of 35 T1WIs were obtained at a temporal resolution of three seconds before and after the injection of Gd-DTPA. Five axial slices covering the tumour were acquired in one series. The baseline T1 map was quantitatively reconstructed using variable flip angles of  $3^\circ$ ,  $6^\circ$ ,  $9^\circ$ ,  $12^\circ$  and  $15^\circ$ .

## Image analysis

The post-processing of MRI data was performed on Advantage Workstation version 4.5 (GE Health Care) by a senior radiologist. DCE-MRI data were analysed using the Cine-tools program. Population-based vascular input function (VIF), as described in a previous study [14], was applied to fit the Tofts model in all animals (VIF = 0.25 in our study). The uptake of contrast agent and VIF for a representative animal is shown in Supplemental Fig. 1. The quantitative parameters, including volume transfer coefficient ( $K_{\text{trans}}$ ), volume fraction of extravascular extracellular space ( $V_e$ ), rate constant of backflux ( $K_{\text{ep}}$ ) and area under the concentration–time curve within the initial 180 s during the first pass of contrast agent ( $\text{AUC}_{180}$ ), were calculated based on the traditional Tofts mathematical model [15], which was originally constructed by generalising existing models for tissues with a negligible amount of intravascular tracer. The equation is as follows:

$$C(t) = K_{\text{trans}} \cdot e^{-tK_{\text{ep}}} * Ca(t).$$

Here, “\*” is convolution, and  $C(t)$  and  $Ca(t)$  are concentration–time curves in the tissue of interest and in the plasma of a feeding artery, respectively.  $K_{\text{ep}}$  is equal to  $K_{\text{trans}}/V_e$ . Unphysiologically relevant voxels (e.g.  $K_{\text{trans}}$  and

$K_{ep} < 0 \text{ min}^{-1}$  or  $> 5 \text{ min}^{-1}$ ,  $V_e < 0$ , or  $> 1$ ,  $AUC_{180} < 0 \text{ mM s}$ ) from the DCE-MRI fitting were removed from subsequent analysis [16]. In the pseudo-colour maps of Figs. 2 and 3, the voxels without a covered colour indicated non-physiological values of  $K_{trans}$ ,  $K_{ep}$ ,  $V_e$  and  $AUC_{180}$ . The approximate percentages of removed voxels for the  $K_{trans}$ ,  $K_{ep}$ ,  $V_e$  and  $AUC_{180}$  maps were 9.8%, 17.8%, 15.3% and 12.7%, respectively.

BOLD-MRI data were used to generate the transverse relaxation rate ( $R2^*$ ) using the Functool-R2Star software. The  $R2^*$  maps were reconstructed by linearly fitting a single exponential model of the  $\ln(\text{signal intensity})$  to the TE curve. The slope of  $\ln(\text{signal intensity})$  versus TE determines  $R2^*$  ( $1/T2^*$ ) value [17]. We referenced T2 WI and delineated the tumour border at the largest cross section as the region of interest (ROI) to measure each quantitative parameter.

### Histological analysis

Fifty-one out of 83 mice were exclusively set for pathological analyses. Three mice were regarded as the common baseline group. Three mice from each pathological subgroup were sampled on days 3, 6, 9 and 12. All of the imaging mice ( $n = 16$ ) were sacrificed for pathologic examinations after the last scanning and corresponded to the result of day 15. The pathologic analyses included haematoxylin and eosin (HE) staining, HIF-1 $\alpha$  immunohistochemical staining, fibronectin, terminal-deoxynucleotidyl transferase mediated dUTP nick end labeling (TUNEL) immunofluorescent staining and  $\alpha$ -smooth muscle actin (SMA) and CD31 immunofluorescent double staining. The excised tumour tissues were fixed in 4% paraformaldehyde, embedded in paraffin, sectioned at a 5- $\mu\text{m}$  thickness and stained with HE following standard procedures. HIF-1 $\alpha$  staining was performed according to the procedures of Li et al. [18]. TUNEL staining was performed to evaluate cell apoptosis using an in situ Cell Death Detection Kit (Roche Diagnostics, Basel, Switzerland) according to the manufacturer's instructions. Fibronectin was incubated with fibronectin antibody (1:200; Abcam, Cambridge, England) and stained with rhodamine-conjugated goat anti-rabbit Ig G (1:300; Proteintech).  $\alpha$ -SMA is a biomarker of pericytes and is associated with vessel maturation [19]. For CD31 and  $\alpha$ -SMA immunofluorescent double staining, a 5- $\mu\text{m}$  cryosection was incubated with an anti-CD31 antibody (1:50, Servicebio, China) for the endothelium and  $\alpha$ -SMA antibody (1:1000; Servicebio, China) for pericyte overnight at 4 °C, which could be used to evaluate vessel maturity. All sections were visualised and recorded using an Olympus BX 53 microscope. Three typical fields on each section ( $\times 200$ ) were selected to calculate the positive staining rate of the cells with the different antibodies using Image-Pro Plus 6.0 software (Media Cybernetics, MD, USA). The vessel

maturity index (VMI) was defined as the ratio of positive  $\alpha$ -SMA to CD31 staining [20].

### Statistical analysis

SPSS 13.0 software (IBM Corporation, Chicago, IL, USA) and GraphPad Prism 5.01 (GraphPad Software Inc., San Diego, CA) were used to perform statistical tests and plot line charts. The numeric results are presented as the mean  $\pm$  standard deviation (SD). The data distribution type was assessed by the Kolmogorov–Smirnov test. Repeated measures analysis of variance was used to analyse the differences in tumour volume,  $K_{trans}$ ,  $V_e$ ,  $K_{ep}$ ,  $AUC_{180}$  and  $R2^*$  values among different time points in each group. To avoid clinically meaningless correlations, this study analysed only the correlation between DCE parameters and CD31 positive staining percentage, VMI value, and the correlation between  $R2^*$  value and HIF-1 $\alpha$ , fibronectin positive staining percentages using Pearson correlation analysis on day 15 in Group B. A  $P$  value  $< 0.05$  was considered statistically significant.

### Results

No obvious abnormal reaction and death occurred in the mice during anti-vascular therapy. We observed tumour growth at each time point and calculated the tumour inhibition rates on day 15. Group D manifested a slower growth trend, smaller tumour volume and higher tumour inhibition rate than the other groups, followed by Groups C, B and A (Fig. 1a). The tumour inhibition rates of Groups B, C and D were 32.3%, 52.0% and 73.4%, respectively.

### MRI results

Conventional MR sequences also showed significantly increased tumour sizes with time in both Groups A and B. The mice in Group B showed no obvious signal changes before day 6 on conventional T1WI, and a small patch of high signal appeared at the periphery and centre of the tumour on days 6 and 9, indicating tumour haemorrhage. On the T2WI, a number of patchy high signals appeared in the tumour core on day 6 to day 15 (Fig. 2). Scattered high signals were also found on T2WI in Group A, but the abnormal signals were not as obvious as those in Group B, and no abnormal signal was found on T1WI (Fig. 3).

The pseudo-colour maps of the  $K_{trans}$ ,  $K_{ep}$ ,  $V_e$  and  $R2^*$  values at each time point in Groups A and B are shown in Figs. 1 and 2. The mean values and trend charts are shown in Tables 1, 2 and Fig. 4. In group B, the  $K_{trans}$  value gradually increased until day 6 after administration, and it showed a downward trend after day 6 and reached the lowest value on day 15 ( $F = 81.386$ ,  $P < 0.001$ ), indicating an increased



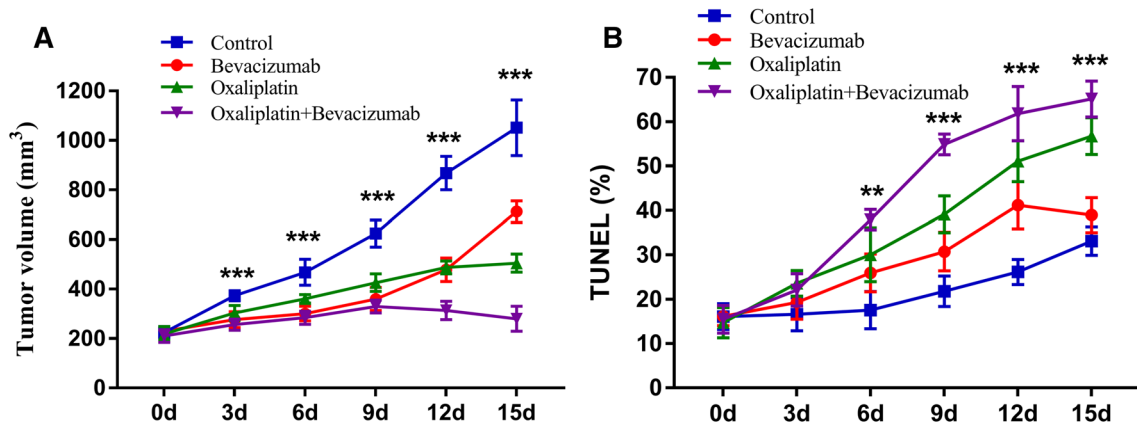


**Fig. 1** Longitudinal assessments of the tumour volumes and TUNEL staining in the four groups. The data are presented as the mean  $\pm$  standard deviation. \* $P < 0.05$ , \*\* $P < 0.01$  and \*\*\* $P < 0.001$  refer to comparisons between groups at corresponding time points using one-way ANOVA

tumour perfusion due to vascular normalization. This trend was reversed by a subsequent anti-angiogenic effect as well as the recession on normalised vascular function.  $V_e$  values decreased with different speeds from 0 to 9 days and fell again on day 15 after a brief increase on day 12 ( $F = 384.290, P < 0.001$ ), indicating a decreased leakage of contrast agent into extravascular extracellular space. The  $K_{ep}$  value gradually increased and reached a peak on day 9, then gradually decreased and returned to the baseline level ( $F = 45.901, P < 0.001$ ), indicating an increased elimination of effusion from the interstitial space and a new balance in the exchange of contrast agent between extravascular and intravascular space. The  $AUC_{180}$  values gradually increased until day 6 and began to decline after a short plateau on day 9 ( $F = 23.514, P < 0.001$ ), indicating that the contrast agent increasingly accumulated in the tumour vessels, which were inhibited afterwards. The trend of the  $R2^*$  value tended to be an inverted triangle, which gradually decreased from 0 to 9 days and then rose after reaching the valley value on day 9 ( $F = 89.323, P < 0.001$ ), indicating an initial relief in tumour hypoxia. However, the trend was reversed due to tumour regrowth and decreased microvessel density. All the results were statistically significant. No statistically significant differences in  $K_{trans}$  ( $F = 0.770, P = 0.576$ ),  $K_{ep}$  ( $F = 0.517, P = 0.762$ ),  $V_e$  ( $F = 0.559, P = 0.731$ ) and  $R2^*$  values ( $F = 1.981, P = 0.101$ ) were found in Group A.

**Histological results**

Representative sections of HE, HIF-1 $\alpha$ , fibronectin, TUNEL and CD31 and  $\alpha$ -SMA double staining from Groups A and B at different time points are shown in Figs. 5 and 6, and the quantitative results from Groups A and B for each parameter are shown in Tables 1, 2 and

Fig. 4. As we merely needed to compare the treatment effects in Groups C and D, only HE and TUNEL staining were performed and are shown in Fig. 7. Their quantitative results are listed in Table 3 and Fig. 4. In Group B, HE staining showed that the tumour cells were densely and disorderly arranged before treatment. The size and morphology of the nucleus varied from one tumour to another, from one location in a tumour to another, and the cytoplasm was filled with mucus. At low magnification, multiple large fat vacuoles were found in the tumour. After bevacizumab administration, HE staining showed an increased necrotic area in the tumour. Nuclear pyknosis, fragmentation, cell debris and homogeneously red-stained cytoplasm could be observed. More obvious necrosis was found in Groups C and D, especially on days 12 and 15. Similar changes were also observed in Group A, but the difference between consecutive time points was non-significant. Quantitatively, Group D, which induced dramatic apoptosis of tumour cells, showed the highest percentage of TUNEL-positive staining on day 15, followed by Groups C, B and A (Fig. 1b).

In the double-stained sections of Group B, green staining of  $\alpha$ -SMA gradually increased 3 days after administration, indicating an increased coverage of pericytes. Quantitative analysis showed that the percentage of red-stained CD31, a marker of microvessel density, showed a transient increasing trend from 0 to 6 days after treatment and then gradually decreased until 15 d ( $F = 17.945, P < 0.001$ ), indicating a delayed anti-angiogenic effect. VMI representing vascular maturity gradually increased from 0 to 9 days and then decreased until day 15 ( $F = 39.867, P < 0.001$ ). The positively stained percentage of fibronectin increased until day 12 and reached a plateau after day 12 ( $F = 64.494, P < 0.001$ ), indicating

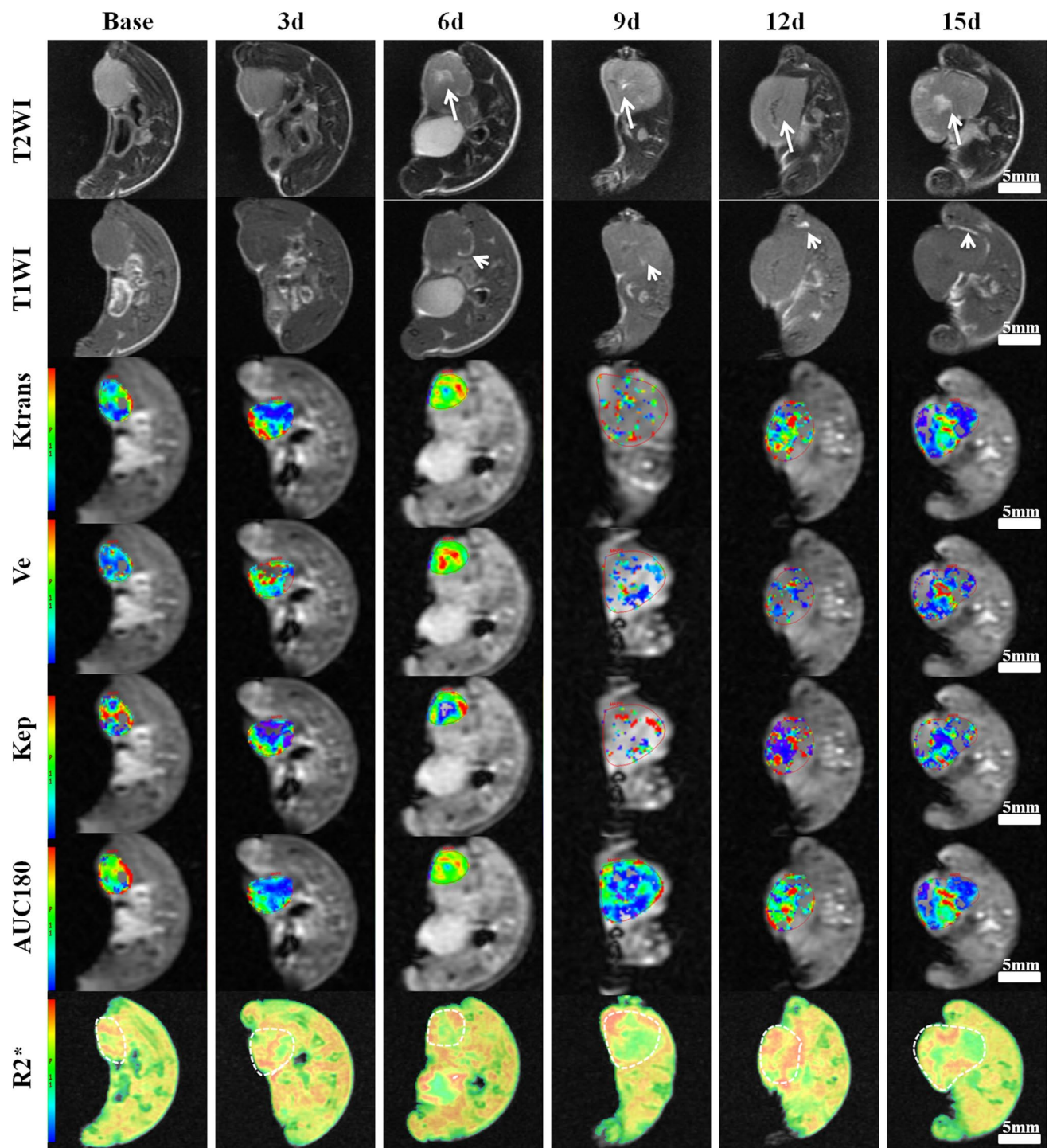


**Fig. 2** Conventional MR sequences (T1WI and T2WI) and pseudo-colour images ( $K_{\text{trans}}$ ,  $V_e$ ,  $K_{\text{ep}}$ ,  $\text{AUC}_{180}$  and  $R2^*$ ) of a representative bevacizumab-treated tumour section (Group B) before and at different time points after the treatment. All images were presented in a two-dimensional axial position. The circles denote tumour areas. The colour ranging from blue to red represents the values ranging from low to high. Scattered high signals were found on days 9 and 15 (T2WI,

arrows). No abnormal signal was found on T1WI.  $K_{\text{trans}}$  ( $\text{min}^{-1}$ ) is the volume transfer coefficient,  $V_e$  is the volume fraction of extravascular extracellular space,  $K_{\text{ep}}$  ( $\text{min}^{-1}$ ) is the rate constant of backflux,  $\text{AUC}_{180}$  is the initial area under the time-signal intensity curve within 180 s of contrast inflow and  $R2^*$  ( $\text{s}^{-1}$ ) is the transverse relaxation rate. The voxels without a covered colour indicated non-physiological values and were excluded from analysis

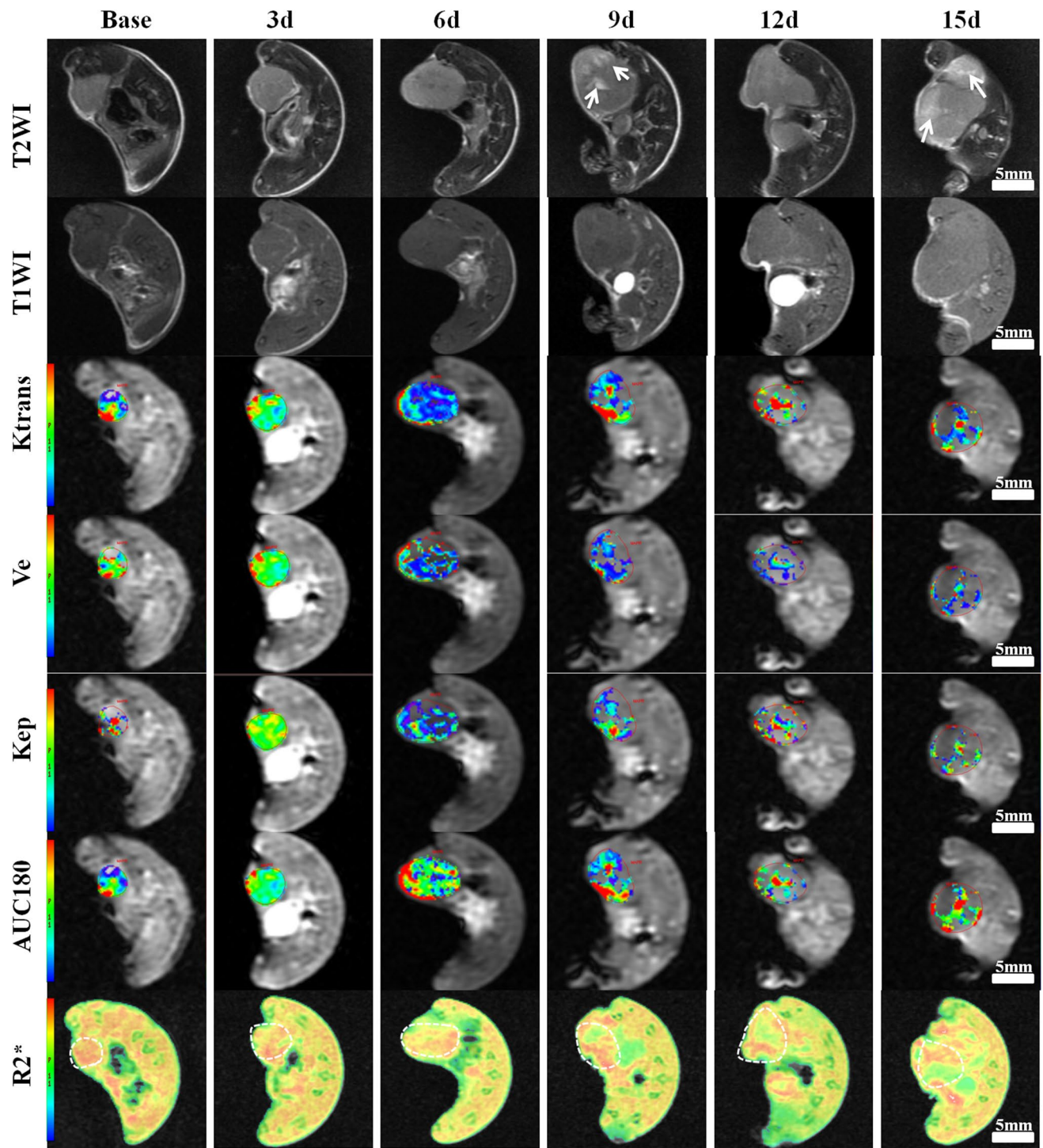


**Fig. 3** Conventional MR sequences (T1WI and T2WI) and pseudo-colour images ( $K_{trans}$ ,  $V_e$ ,  $K_{ep}$ ,  $AUC_{180}$  and  $R2^*$ ) of a representative saline-treated tumour section (Group A) before and at different time points after the treatment. All images were presented in a two-dimensional axial position. The circles denote tumour areas. The colour ranging from blue to red represents the values ranging from low to high. A small patch of high signal appeared at the periphery and centre of the tumour on days 6 and 9, indicating tumour haemorrhage

(T1WI, arrowheads). A number of patchy areas of high-signal areas appear in the tumour core on day 6 to day 15 (T2WI, arrows).  $K_{trans}$  ( $\text{min}^{-1}$ ) is the volume transfer coefficient,  $V_e$  is the volume fraction of extravascular extracellular space,  $K_{ep}$  ( $\text{min}^{-1}$ ) is the rate constant of backflux,  $AUC_{180}$  is the initial area under the time-signal intensity curve within 180 s of contrast inflow and  $R2^*$  ( $\text{s}^{-1}$ ) is the transverse relaxation rate. The voxels without a covered colour indicated non-physiological values and were excluded from analysis



**Table 1** The quantitative results of MRI-derived parameters, pathological indicators and tumour volume in Group A

Group A	Base	3 days	6 days	9 days	12 days	15 days	<i>F</i>	<i>P</i>
R2*(s <sup>-1</sup> )	25.388 ± 1.122	26.075 ± 1.036	25.088 ± 0.779	24.700 ± 1.218	24.513 ± 1.745	24.375 ± 1.537	1.981	0.101
<i>K</i> <sub>trans</sub> (min <sup>-1</sup> )	0.138 ± 0.005	0.147 ± 0.008	0.142 ± 0.009	0.145 ± 0.011	0.146 ± 0.012	0.145 ± 0.015	0.77	0.576
<i>V</i> <sub>e</sub>	0.587 ± 0.083	0.610 ± 0.059	0.578 ± 0.047	0.614 ± 0.042	0.619 ± 0.058	0.603 ± 0.070	0.559	0.731
<i>K</i> <sub>ep</sub> (min <sup>-1</sup> )	0.754 ± 0.034	0.739 ± 0.069	0.770 ± 0.029	0.764 ± 0.040	0.749 ± 0.045	0.749 ± 0.045	0.517	0.762
AUC <sub>180</sub> (mM s)	0.785 ± 0.032	0.778 ± 0.040	0.766 ± 0.030	0.752 ± 0.036	0.770 ± 0.057	0.779 ± 0.046	0.654	0.660
CD31 (%)	38.2 ± 3.8	36.1 ± 3.7	40.6 ± 3.7	42.6 ± 3.2	38.1 ± 3.4	40.7 ± 2.9	1.645	0.202
VMI (%)	54.2 ± 1.6	46.1 ± 3.2	53.2 ± 4.4	47.8 ± 4.9	50.7 ± 3.1	48.0 ± 3.3	2.871	0.050
HIF-1a (%)	39.3 ± 5.6	38.4 ± 2.6	40.6 ± 2.6	40.6 ± 2.8	43.9 ± 2.3	39.7 ± 3.5	0.937	0.482
Fibronectin(%)	23.6 ± 3.0	22.4 ± 4.2	20.8 ± 5.7	18.6 ± 4.4	20.2 ± 4.1	21.2 ± 3.8	0.564	0.726
TUNEL (%)	16.1 ± 2.9	16.6 ± 3.8	17.5 ± 4.2	21.8 ± 3.5	26.1 ± 2.9	33.1 ± 3.2	20.697	<b>0.001</b>
Tumour volume (mm <sup>3</sup> )	224.9 ± 23.5	373.0 ± 20.3	467.8 ± 52.4	624.3 ± 54.5	867.8 ± 67.3	1051.3 ± 112.3	195.697	<b>0.001</b>

The *P* values are generalised from repeated measures analysis of variance among different time points in each group

**Table 2** The quantitative results of MRI-derived parameters, pathological indicators and tumour volume in Group B

Group B	Base	3 days	6 days	9 days	12 days	15 days	<i>F</i>	<i>P</i>
R2*(s <sup>-1</sup> )	24.813 ± 0.961	24.675 ± 1.070	21.425 ± 1.371	17.850 ± 0.885	24.613 ± 0.640	27.013 ± 0.734	89.323	<b>0.001</b>
<i>K</i> <sub>trans</sub> (min <sup>-1</sup> )	0.135 ± 0.005	0.147 ± 0.006	0.175 ± 0.009	0.161 ± 0.006	0.140 ± 0.005	0.116 ± 0.008	81.386	<b>0.001</b>
<i>V</i> <sub>e</sub>	0.652 ± 0.006	0.559 ± 0.026	0.466 ± 0.016	0.286 ± 0.027	0.363 ± 0.020	0.246 ± 0.033	384.290	<b>0.001</b>
<i>K</i> <sub>ep</sub> (min <sup>-1</sup> )	0.788 ± 0.030	0.804 ± 0.036	0.983 ± 0.059	1.105 ± 0.091	0.840 ± 0.047	0.786 ± 0.041	45.901	<b>0.001</b>
AUC <sub>180</sub> (mM s)	0.823 ± 0.043	0.907 ± 0.052	1.125 ± 0.130	1.128 ± 0.163	0.887 ± 0.061	0.731 ± 0.040	23.514	<b>0.001</b>
CD31 (%)	36.7 ± 5.1	50.5 ± 01.7	56.7 ± 4.8	45.8 ± 2.0	32.1 ± 6.4	29.8 ± 5.9	17.945	<b>0.001</b>
VMI (%)	55.6 ± 2.0	55.7 ± 1.7	65.3 ± 2.8	81.5 ± 6.8	65.9 ± 2.8	52.1 ± 2.6	39.867	<b>0.001</b>
HIF-1a (%)	43.1 ± 2.9	51.6 ± 5.1	41.4 ± 1.2	30.4 ± 4.2	31.9 ± 4.0	50.0 ± 3.1	24.356	<b>0.001</b>
Fibronectin (%)	21.3 ± 4.5	31.4 ± 3.2	43.6 ± 4.4	49.2 ± 4.3	61.4 ± 3.6	59.6 ± 3.4	64.494	<b>0.001</b>
TUNEL (%)	16.1 ± 2.1	19.3 ± 3.8	25.9 ± 4.3	30.7 ± 4.4	41.2 ± 5.3	38.9 ± 3.9	24.099	<b>0.001</b>
Tumour volume (mm <sup>3</sup> )	229.5 ± 22.7	276.9 ± 32.1	300.9 ± 29.7	359.8 ± 46.5	478.3 ± 47.7	712.3 ± 43.3	174.648	<b>0.001</b>

The *P* values are generalised from repeated measures analysis of variance among different time points in each group

an increased synthesis of extracellular matrix. The positively stained percentage of HIF-1α, which characterises the degree of hypoxia, increased briefly after administration, then gradually decreased from 3 to 9 days, and rose again after a short plateau of 9–12 days (*F* = 24.356, *P* < 0.001). There was no significant trend in each indicator of Group A (*P* > 0.05).

### Correlation results

The R2\* value showed positive correlations with HIF-1α (*r* = 0.810, *P* = 0.015) and fibronectin positive staining rate (*r* = 0.816, *P* = 0.013). The Pearson correlation coefficients and *P* values between *K*<sub>trans</sub> and CD31 were *r* = 0.854, *P* = 0.007; *K*<sub>trans</sub> and VMI were *r* = 0.795, *P* = 0.018; *V*<sub>e</sub> and CD31 were *r* = 0.744, *P* = 0.034; *V*<sub>e</sub> and VMI were *r* = 0.712, *P* = 0.048; *K*<sub>ep</sub> and CD31 were *r* = 0.729, *P* = 0.040; *K*<sub>ep</sub> and VMI were *r* = 0.758, *P* = 0.029; AUC<sub>180</sub> and CD31 were *r* = 0.750, *P* = 0.032; AUC<sub>180</sub> and VMI were *r* = 0.808,

*P* = 0.015. *K*<sub>trans</sub> showed the strongest correlation with CD31, while the R2\* value was more closely correlated with fibronectin staining.

### Discussion

Angiogenesis plays an important role in tumourigenesis, providing nutrients for its growth and passage for distant metastasis. The concept of “anti-tumour angiogenesis” was initially proposed by Professor Folkman in 1971. However, the treatment efficacies of anti-angiogenesis monotherapy were not as ideal as expected [6, 21]. In contrast to previous clinical studies, our study aimed to explore microenvironmental changes, including microcirculation perfusion and tumour invasiveness, during anti-angiogenesis treatment with more objective imaging techniques and the potential effect of bevacizumab on



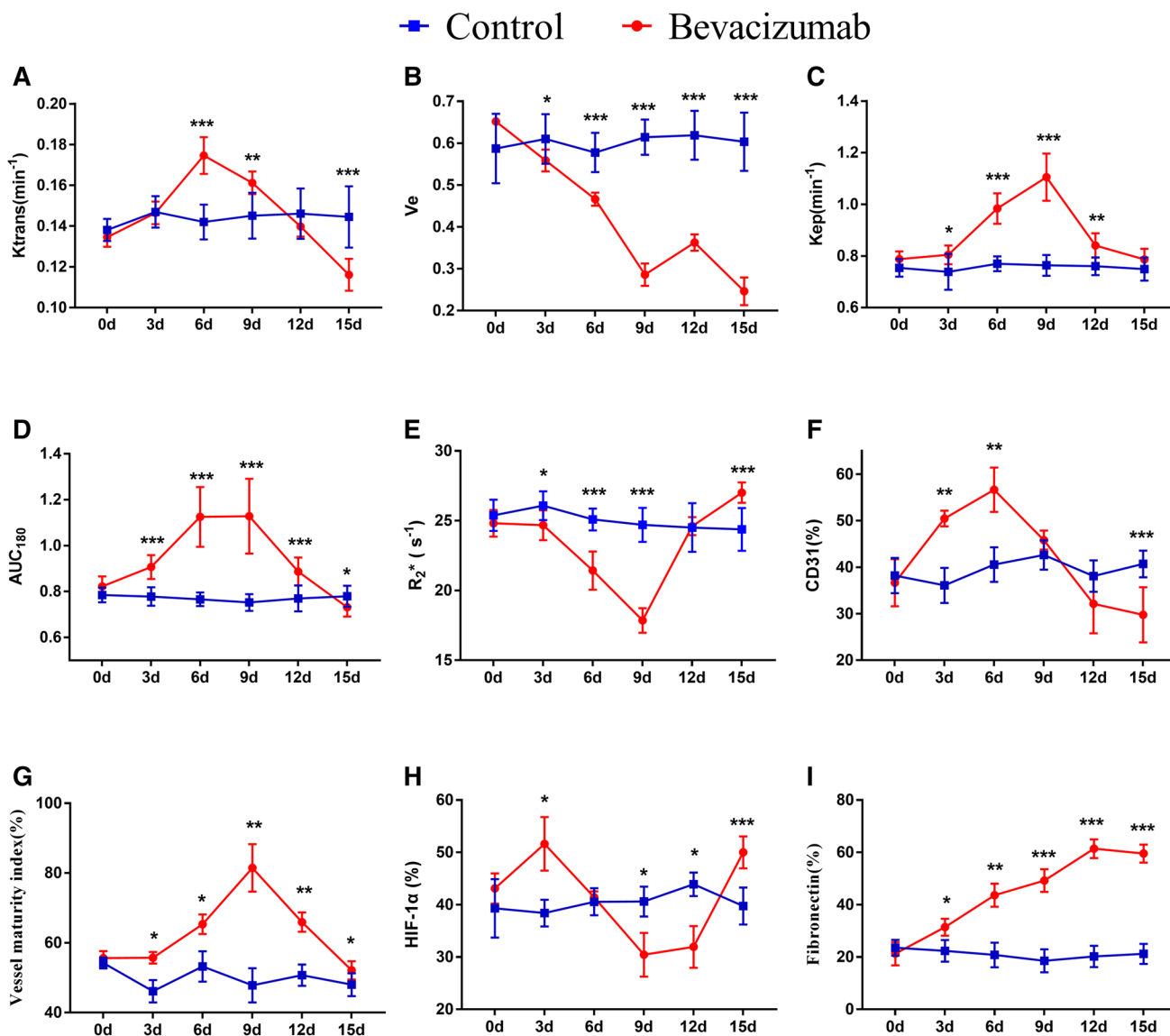


**Fig. 4** Longitudinal assessments of the MRI parameters and pathological indicators in Group A (blue lines) and Group B (red lines). Data points are plotted as the mean  $\pm$  standard deviation. \* $P < 0.05$ ,

\*\* $P < 0.01$  and \*\*\* $P < 0.001$  refer to comparisons between Groups A and B at respective time points using two independent-samples  $t$  test

conventional chemotherapy. Our results showed a good response to current issues.

In our study, although monotherapy with bevacizumab or oxaliplatin manifested a certain inhibitory effect on tumour growth compared with the control group, the tumour still maintained a steady growth tendency after treatment. However, the growth trend was significantly inhibited or even reversed in Group D. TUNEL staining also confirmed that a larger area of cell apoptosis appeared in the tumour during combination therapy, compared with other groups.

Previous research mainly confirmed the vascular normalization process via pathological examinations in animal models [22], but this approach is not suitable for

continuous clinical monitoring, and the structural changes may lag behind functional changes. In a previous study, Shi et al. [23] observed the therapeutic response of a vascular disrupting agent (VDA) (combretastatin A4 phosphate) on a non-small cell lung cancer xenograft model using functional DCE-MRI and found that the  $K_{trans}$  value had a good predictive value in the acute vascular disrupting effect and short-term efficacy. Therefore, we also used DCE-MRI to evaluate the anti-tumour effect of anti-angiogenic agents and found that  $K_{trans}$  gradually increased within 6 days after bevacizumab administration.  $K_{trans}$  is related to microcirculation perfusion and microvascular permeability. Previous studies have reported that

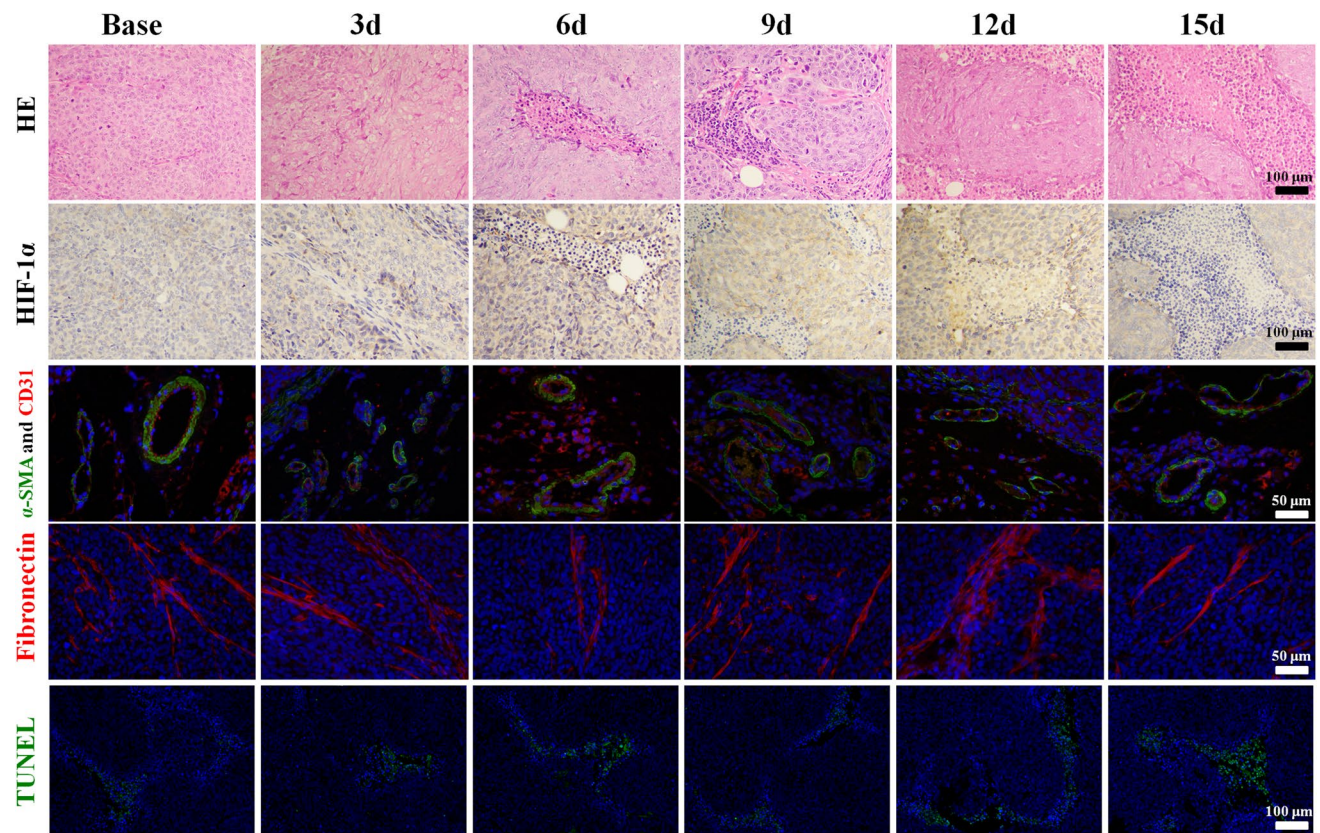


**Fig. 5** Representative HE ( $\times 100$ ), HIF-1 $\alpha$  ( $\times 100$ ),  $\alpha$ -SMA/CD31 ( $\times 200$ ), fibronectin ( $\times 200$ ) and TUNEL staining ( $\times 100$ ) at baseline and at different time points after the treatment in Group A. The

nucleus was stained in blue,  $\alpha$ -SMA in green and CD31 in red. Apoptosis was manifested in green in TUNEL staining and fibronectin in red in fibronectin staining

anti-angiogenic agents can promote the proliferation of pericytes and repair of the basement membrane of tumour vessels, which can reduce the high permeability level of newborn microvessels, promote vessel maturation and temporarily normalise vessel function [24, 25]. Therefore, the leakage of contrast agent is reduced, causing an increase in tumour perfusion as well as the  $K_{trans}$  value. This may also help to reduce the interstitial fluid pressure and improve drug delivery.  $K_{trans}$  showed a downward trend after day 6 and reached the lowest value on day 15. It is speculated that inhibition of neovascularization may lead to a subsequent decrease in the overall microcirculation perfusion, and the decrease in vascular permeability led to a reduction in the exchange of contrast agent and  $K_{trans}$  value.  $V_e$  mainly showed a decreasing trend until day 15 but transiently increased on days 9 to 12 after treatment. Except for the effect of vascular normalization, the volume fraction of contrast agent accumulating in extravascular extracellular space increases with decreased tumour cellularity and interstitial fluid pressure due to an increased area of tumour necrosis after anti-angiogenic treatment. The  $\alpha$ -SMA and CD31 double staining also confirmed the increase in pericyte coverage and decrease in microvessel

density during anti-vascular treatment.  $AUC_{180}$  is another valuable parameter that can semiquantitatively measure the accumulated exchange amount of contrast agent delivering to extravascular space from tumour vessels. It manifested a slow increase until day 6 and began to decline after a short plateau on day 9, indicating an increase in blood supply on days 3 to 9. This further confirmed the reparation of vessel function, which may increase the oxaliplatin delivery in Group D. In addition, we found that  $K_{trans}$ ,  $K_{ep}$ ,  $AUC_{180}$  and VMI values were higher than their baseline values on days 3–12, which provided a certain reference to determine the range of vascular normalization. However, the results were inconsistent with the time ranges reported in a previous study (2–6 days after administration) [26]. We speculated that the observation time was not long enough, and only a single dose of bevacizumab was applied, which cannot guarantee a persistent and stable drug concentration in a previous study. However, we intermittently applied a low dose of bevacizumab five times in this study. The DCE-MRI showed a longer vascular normalization process, indicating that the time range was not constant. A previous study reported that excess VEGF-A disrupted pericyte recruitment and interfered with vascular development [27].



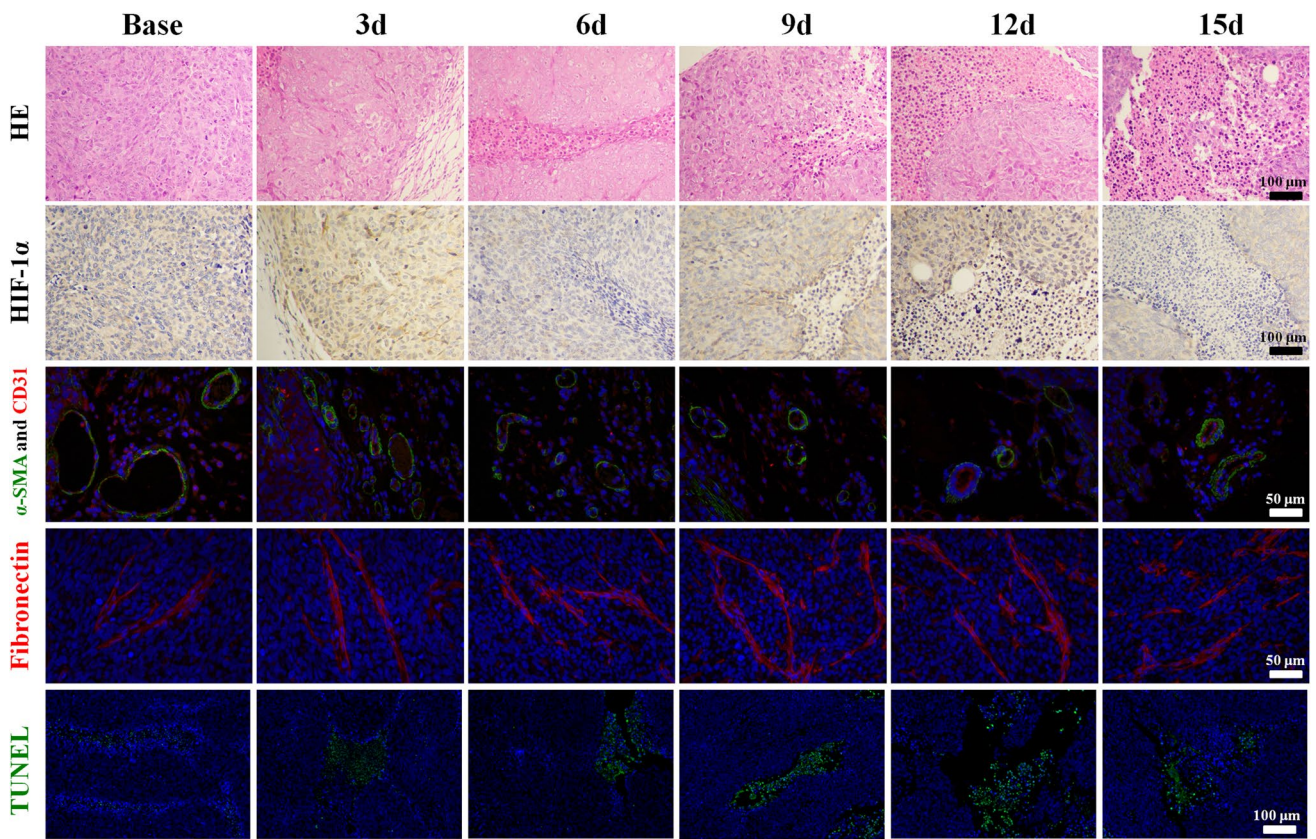


**Fig. 6** Representative HE ( $\times 100$ ), HIF-1 $\alpha$  ( $\times 100$ ),  $\alpha$ -SMA/CD31 ( $\times 200$ ), fibronectin ( $\times 200$ ) and TUNEL staining ( $\times 100$ ) at baseline and at different time points after the treatment in Group B. The

nucleus was stained in blue,  $\alpha$ -SMA in green and CD31 in red. Apoptosis was manifested in green in TUNEL staining and fibronectin in red in fibronectin staining

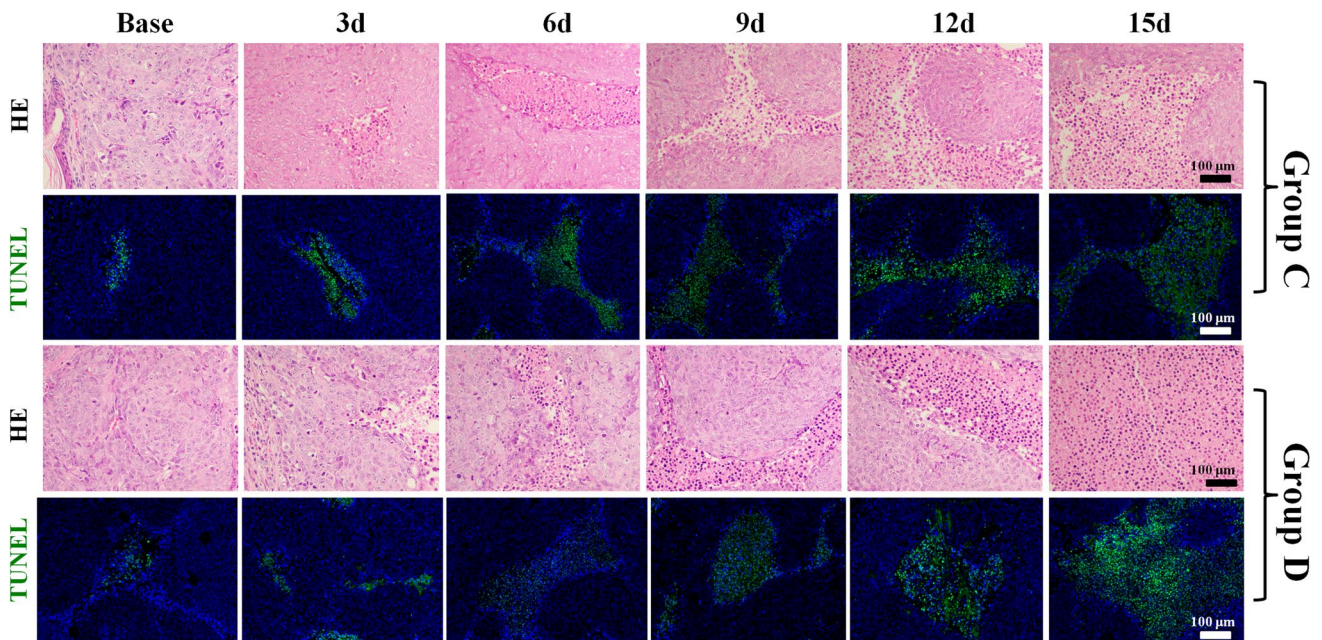


**Fig. 7** Representative HE ( $\times 100$ ) and TUNEL staining ( $\times 100$ ) at baseline and at different time points after the treatment in Groups C and D. Apoptosis cells are shown in green in TUNEL staining

**Table 3** The TUNEL-positive staining results and tumour volumes in Group C and D

	Group C		Group D	
	TUNEL (%)	Tumour volume (mm <sup>3</sup> )	TUNEL (%)	Tumour volume (mm <sup>3</sup> )
Base	14.7 ± 3.4	218.5 ± 29.6	15.5 ± 3.1	210.0 ± 25.9
3 days	23.6 ± 2.9	303.4 ± 30.1	22.1 ± 3.7	256.0 ± 22.2
6 days	30.0 ± 6.1	360.5 ± 16.9	37.9 ± 2.3	284.0 ± 26.1
9 days	39.1 ± 4.2	425.9 ± 35.8	54.9 ± 2.3	329.2 ± 26.1
12 days	51.1 ± 4.6	487.1 ± 26.0	61.8 ± 6.1	313.3 ± 37.1
15 days	56.7 ± 4.1	504.9 ± 36.3	65.1 ± 4.0	279.9 ± 50.4
<i>F</i>	61.633	110.4	113.813	13.414
<i>P</i>	0.001	0.001	0.001	0.001

The *P* values are generalised from repeated measures analysis of variance among different time points in each group

In our study, we found that bevacizumab can increase pericyte coverage and vessel maturity. Rational application of bevacizumab could balance the anti-angiogenic effect and vascular normalization phenomenon that helped for longer effective reaction times of chemotherapy. The  $K_{trans}$  value showed stronger correlations with CD31 and VMI values with more consistent trends compared with the  $K_{ep}$ ,  $V_e$  and  $AUC_{180}$  values, suggesting that  $K_{trans}$  is a better imaging indicator in reflecting vessel maturity and predicting the vascular normalization process.

Hypoxia is an important reason for chemoradiotherapy resistance. Detection of hypoxia and improvement of the hypoxic microenvironment are important issues for anti-tumour treatment. In a recent study, Liang et al. [28] investigated the therapeutic efficacy of another VDA (desacetylvinblastine monohydrate) on a hepatocarcinoma xenograft model using BOLD-MRI and found that  $R2^*$  had a close relationship with tumour hypoxia during VDA treatment. Therefore, BOLD-MRI was also applied to evaluate the oxygen metabolism after anti-vascular treatment and found that the  $R2^*$  value gradually decreased within 9 days after treatment and reversed after reaching the valley value on day 9. The initial decrease in the  $R2^*$  value was mainly due to the vascular normalization effect of bevacizumab, which temporarily increased tumour perfusion and relieved tumour hypoxia. Afterwards, inhibition of angiogenesis and tumour regrowth contributed to tumour hypoxia and an increased  $R2^*$  value. The timing that  $R2^*$  rose was different from previous studies [28]. The reason was mainly due to the hyperacute disrupting effect of VDAs that can rapidly destroy the pre-existing vasculature in the tumour, whereas bevacizumab merely inhibits neovascularization. In addition, the  $R2^*$  value showed a good correlation and a relatively consistent trend with HIF-1 $\alpha$ , suggesting that the  $R2^*$  value could predict tumour hypoxia during anti-angiogenic therapy. The synergistic effect of bevacizumab in tumour chemotherapy may

also be attributed to improved tumour hypoxia from day 3 to day 12, which was detected by BOLD-MRI.

In our study, the positive percentage of fibronectin, a major component of the tumour microenvironment and biomarker of epithelial–mesenchymal transition [29], gradually increased and reached a plateau on day 12 after bevacizumab treatment. The  $\alpha5\beta1$  integrin is a specific receptor of fibronectin on the surface of tumour cells. When the expression of fibronectin increases, the adhesion between tumour cells and extracellular matrix is enhanced, restricting cell migration and metastasis [30]. In the current study, we found that bevacizumab can improve tumour perfusion and relieve hypoxia by temporarily normalising the vascular structure and function, promoting the synthesis of fibronectin in the extracellular matrix. It did not degrade rapidly with changes in the microenvironment, and the cumulative effect contributed to an upward trend after treatment. The  $R2^*$  value showed a positive correlation with fibronectin, suggesting that it can also be used to assess tumour invasiveness during anti-vascular treatment.

There were still some limitations in this study. First, to ensure the consistency of MRI examinations, we set up another parallel group for pathological comparison, and the correspondence between MR parameters and pathological findings decreased to a certain extent. Second, continuous contrast-enhanced imaging in the short term required multiple injections of contrast agents, which posed a certain risk to the organism. Third, we had not performed IVIM-DWI and had not compared its diagnostic performance with that DCE-MRI; it remains unclear which imaging sequence is superior for predicting the vascular normalization process. Finally, we did not calculate the tumour cellularity and performed a correlation analysis with  $V_e$  due to a low-colour contrast between the necrotic area and the viable area in our HE staining. The credibility of interpretation in  $V_e$  decreased to a certain extent.

In conclusion, bevacizumab can improve pericyte coverage and temporarily increase tumour perfusion by



normalising vessel structures and function. Intermittent application of low-dose angiogenesis inhibitors will not strongly inhibit neovascularization but will prolong the vascular normalization process and relieve tumour hypoxia. We found that bevacizumab monotherapy was not sufficient to inhibit tumour growth and was effective only if combined with oxaliplatin, which significantly enhanced its anti-tumour efficacy. The fact that the effect is synergistic rather than additive may result from an increase in drug delivery and relief in hypoxia-related treatment resistance, the mechanisms of which were confirmed by DCE-MRI and BOLD-MRI in our study.  $K_{trans}$  was closely correlated with tumour perfusion and vessel permeability, which is the best imaging marker to evaluate vessel maturity and determine the vascular normalization process, while  $R2^*$  has a higher predictive value in tumour hypoxia and metastatic potential during anti-vascular treatment.

**Acknowledgements** This work was supported by Science and Technology Planning Project of Guangdong Province [Grant Number 2017A020215065], Key Program of Natural Science Foundation of Guangdong Province of China [Grant Number 2018B0303110011], National Natural Science Foundation of China [Grant Number 21317241], Guangzhou Key Laboratory of Molecular and Functional Imaging for Clinical Translation [Grant Number 201905010003] and Engineering Research Center of Medical Imaging Artificial Intelligence for Precision Diagnosis and Treatment, Guangdong Province.

## Compliance with ethical standards

**Conflict of interest** The authors have stated explicitly that there are no conflicts of interest in connection with this article.

## References

- Jain RK, Di Tomaso E, Duda DG et al (2007) Angiogenesis in brain tumours. *Nat Rev Neurosci* 8:610–622. <https://doi.org/10.1038/nrn2175>
- Huang Y, Lin D, Taniguchi CM (2017) Hypoxia inducible factor (HIF) in the tumor microenvironment: friend or foe? *Sci China Life Sci* 60:1114–1124. <https://doi.org/10.1007/s11427-017-9178-y>
- Xiong H, Yin P, Li X et al (2019) The features of cerebral permeability and perfusion detected by dynamic contrast-enhanced magnetic resonance imaging with Patlak model in relapsing-remitting multiple sclerosis. *Ther Clin Risk Manag* 15:233–240. <https://doi.org/10.2147/TCRM.S189598>
- Yeldag G, Rice A, Del Rio Hernandez A (2018) Chemoresistance and the self-maintaining tumor microenvironment. *Cancers (Basel)* 10:E471. <https://doi.org/10.3390/cancers10120471>
- Diaz RJ, Ali S, Qadir MG et al (2017) The role of bevacizumab in the treatment of glioblastoma. *J Neurooncol* 133:455–467. <https://doi.org/10.1007/s11060-017-2477-x>
- Viallard C, Larrivee B (2017) Tumor angiogenesis and vascular normalization: alternative therapeutic targets. *Angiogenesis* 20:409–426. <https://doi.org/10.1007/s10456-017-9562-9>
- Pan JH, Zhu S, Huang J et al (2018) Monitoring the process of endostar-induced tumor vascular normalization by non-contrast intravoxel incoherent motion diffusion-weighted MRI. *Front Oncol* 8:524. <https://doi.org/10.3389/fonc.2018.00524>
- Choi YJ, Lee IS, Song YS et al (2019) Diagnostic performance of diffusion-weighted (DWI) and dynamic contrast-enhanced (DCE) MRI for the differentiation of benign from malignant soft-tissue tumors. *J Magn Reson Imaging*. <https://doi.org/10.1002/jmri.26607>
- Wu C, Pineda F, Hormuth DA 2nd et al (2019) Quantitative analysis of vascular properties derived from ultrafast DCE-MRI to discriminate malignant and benign breast tumors. *Magn Reson Med* 81:2147–2160. <https://doi.org/10.1002/mrm.27529>
- Cao J, Pickup S, Clendenin C et al (2018) Dynamic contrast-enhanced MRI detects responses to stroma-directed therapy in mouse models of pancreatic ductal adenocarcinoma. *Clin Cancer Res*. <https://doi.org/10.1158/1078-0432.ccr-18-2276>
- Zhou H, Belzile O, Zhang Z et al (2019) The effect of flow on blood oxygen level dependent ( $R2^*$ ) MRI of orthotopic lung tumors. *Magn Reson Med*. <https://doi.org/10.1002/mrm.27661>
- Bonetti A, Giuliani J, Muggia F (2014) Targeted agents and oxaliplatin-containing regimens for the treatment of colon cancer. *Anticancer Res* 34:423–434
- Huang Y, Yuan J, Righi E et al (2012) Vascular normalizing doses of antiangiogenic treatment reprogram the immunosuppressive tumor microenvironment and enhance immunotherapy. *Proc Natl Acad Sci USA* 109:17561–17566. <https://doi.org/10.1073/pnas.1215397109>
- Loveless ME, Halliday J, Liess C et al (2012) A quantitative comparison of the influence of individual versus population-derived vascular input functions on dynamic contrast enhanced-MRI in small animals. *Magn Reson Med* 67:226–236. <https://doi.org/10.1002/mrm.22988>
- Tofts PS, Brix G, Buckley DL et al (1999) Estimating kinetic parameters from dynamic contrast-enhanced T(1)-weighted MRI of a diffusible tracer: standardized quantities and symbols. *J Magn Reson Imaging* 10:223–232
- Syed AK, Woodall R, Whisenant JG et al (2019) characterizing trastuzumab-induced alterations in intratumoral heterogeneity with quantitative imaging and immunohistochemistry in HER2+ breast cancer. *Neoplasia* 21:17–29. <https://doi.org/10.1016/j.neo.2018.10.008>
- Robinson SP, Rodrigues LM, Howe FA et al (2001) Effects of different levels of hypercapnic hyperoxia on tumour  $R2^*$  and arterial blood gases. *Magn Reson Imaging* 19:161–166. [https://doi.org/10.1016/S0730-725x\(01\)00230-2](https://doi.org/10.1016/S0730-725x(01)00230-2)
- Li F, Lee KE, Simon MC (2018) Detection of hypoxia and HIF in paraffin-embedded tumor tissues. *Methods Mol Biol* 1742:277–282. [https://doi.org/10.1007/978-1-4939-7665-2\\_24](https://doi.org/10.1007/978-1-4939-7665-2_24)
- Alarcon-Martinez L, Yilmaz-Ozcan S, Yemisci M et al (2018) Capillary pericytes express alpha-smooth muscle actin, which requires prevention of filamentous-actin depolymerization for detection. *Elife* 7:e34861. <https://doi.org/10.7554/eLife.34861>
- Eberhard A, Kahlert S, Goede V et al (2000) Heterogeneity of angiogenesis and blood vessel maturation in human tumors: implications for antiangiogenic tumor therapies. *Cancer Res* 60:1388–1393
- Roodink I, Leenders WP (2010) Targeted therapies of cancer: angiogenesis inhibition seems not enough. *Cancer Lett* 299:1–10. <https://doi.org/10.1016/j.canlet.2010.09.004>
- Li N, Zheng D, Wei X et al (2012) Effects of recombinant human endostatin and its synergy with cisplatin on circulating endothelial cells and tumor vascular normalization in A549 xenograft murine model. *J Cancer Res Clin Oncol* 138:1131–1144. <https://doi.org/10.1007/s00432-012-1189-z>

23. Shi C, Liu D, Xiao Z et al (2017) Monitoring tumor response to antivascular therapy using non-contrast intravoxel incoherent motion diffusion-weighted MRI. *Cancer Res* 77:3491–3501. <https://doi.org/10.1158/0008-5472.CAN-16-2499>
24. El Alaoui-Lasmali K, Faivre B (2018) Antiangiogenic therapy: markers of response, “normalization” and resistance. *Crit Rev Oncol Hematol* 128:118–129. <https://doi.org/10.1016/j.critrevonc.2018.06.001>
25. Raza A, Franklin MJ, Dudek AZ (2010) Pericytes and vessel maturation during tumor angiogenesis and metastasis. *Am J Hematol* 85:593–598. <https://doi.org/10.1002/ajh.21745>
26. Yang J, Liao C, Liu Y et al (2018) MR imaging biomarkers evaluating vascular normalization window after anti-vessel treatment. *Oncotarget* 9:11964–11976. <https://doi.org/10.18632/oncotarget.22600>
27. Darden J, Payne LB, Zhao H et al (2019) Excess vascular endothelial growth factor-A disrupts pericyte recruitment during blood vessel formation. *Angiogenesis* 22:167–183. <https://doi.org/10.1007/s10456-018-9648-z>
28. Liang J, Ma R, Chen H et al (2019) Detection of hyperacute reactions of desacetylvinblastine monohydrate in a xenograft model using intravoxel incoherent motion DWI and R2\* mapping. *AJR Am J Roentgenol* 212:717–726. <https://doi.org/10.2214/ajr.18.20517>
29. Griggs LA, Hassan NT, Malik RS et al (2017) Fibronectin fibrils regulate TGF-beta1-induced epithelial–mesenchymal transition. *Matrix Biol* 60–61:157–175. <https://doi.org/10.1016/j.matbio.2017.01.001>
30. Oudin MJ, Jonas O, Kosciuk T et al (2016) Tumor cell-driven extracellular matrix remodeling drives haptotaxis during metastatic progression. *Cancer Discov* 6:516–531. <https://doi.org/10.1158/2159-8290.CD-15-1183>

**Publisher's Note** Springer Nature remains neutral with regard to jurisdictional claims in published maps and institutional affiliations.

## Affiliations

Jianye Liang<sup>1</sup> · Qingqing Cheng<sup>1</sup> · Jiayi Huang<sup>1</sup> · Mengjie Ma<sup>1</sup> · Dong Zhang<sup>1</sup> · Xueping Lei<sup>3</sup> · Zeyu Xiao<sup>1</sup> · Dongmei Zhang<sup>2</sup> · Changzheng Shi<sup>1</sup> · Liangping Luo<sup>1</sup> 

Jianye Liang  
ljygnu@foxmail.com

Qingqing Cheng  
15089813225@163.com

Jiayi Huang  
jiaxihuangjessie@foxmail.com

Mengjie Ma  
xyz8384@163.com

Dong Zhang  
lbzhangdong@126.com

Xueping Lei  
xuepinglei@foxmail.com

Zeyu Xiao  
zeyuxiao@jnu.edu.cn

- <sup>1</sup> Medical Imaging Center, The First Affiliated Hospital of Jinan University, No.613, Huangpu Road West, Tianhe District, Guangzhou 510630, Guangdong Province, China
- <sup>2</sup> College of Pharmacy, Jinan University, 601 Huangpu Road West, Guangzhou 510632, Guangdong, China
- <sup>3</sup> Key Laboratory of Molecular Target and Clinical Pharmacology, School of Pharmaceutical Sciences & Fifth Affiliated Hospital, Guangzhou Medical University, Guangzhou, Guangdong 511436, China